

The 54 days orbital period of AX J1820.5–1434 unveiled by Swift.

A. Segreto¹, V. La Parola¹, G. Cusumano, A. D’Ai², N. Masetti³, S. Campana⁴

¹ INAF - Istituto di Astrofisica Spaziale e Fisica Cosmica di Palermo, Via U. La Malfa 153, 90146 Palermo, Italy

² Dipartimento di Fisica e Chimica, Università di Palermo, via Archirafi 36, 90123, Palermo, Italy

³ INAF - Istituto di Astrofisica Spaziale e Fisica Cosmica di Bologna, via Gobetti 101, 40129, Bologna, Italy

⁴ INAF - Brera Astronomical Observatory, via Bianchi 46, 23807, Merate (LC), Italy

Preprint online version: June 4, 2018

ABSTRACT

Context. The hard X-ray survey that Swift-BAT has been performing since late 2004 has provided a considerable database for a large number of sources whose hard X-ray emission was poorly known.

Aims. We are exploiting the BAT survey archive to improve the temporal and spectral characterization of the Galactic hard-X-ray sources. In this letter we focus on the study of the high mass X-ray binary AX J1820.5–1434.

Methods. All the data relevant to AX J1820.5–1434 have been extracted from the BAT survey archive and analyzed using a folding technique to search for periodical modulations. A broad-band spectral analysis was also performed complementing the BAT spectrum with the available Swift-XRT and XMM-Newton pointed observations.

Results. A timing analysis has revealed the detection of a coherent signal at $P_0 = 54.0 \pm 0.4$ d, that we interpret as the orbital period of the binary system. When folded with a period of P_0 , the light curve shows an asymmetric profile, with a minimum roughly consistent with zero intensity. The broad band spectral analysis performed coupling Swift-XRT, XMM-Newton and Swift-BAT spectra confirms that the source emission is well modeled with a strongly absorbed power law with no evidence for a high energy exponential cutoff.

Key words. X-rays: general - : data analysis - stars: neutron - X-rays: individuals: AX J1820.5–1434

1. Introduction

Since November 2004 the Burst Alert Telescope (BAT, Barthelmy et al. 2005) on board Swift (Gehrels et al. 2004) has been performing a continuous monitoring of the sky in the hard X-ray domain (15–150 keV). Thanks to its large field of view (1.4 steradian half coded) and to its pointing strategy, BAT covers a fraction of the sky of 50% to 80% every day. This monitoring has been very successful to unveil the binary nature of many Galactic sources (e.g. Corbet & Krimm 2009; Corbet et al. 2010a; Cusumano et al. 2010; La Parola et al. 2010; D’Ai et al. 2011).

In this Letter we present a temporal and spectral analysis of the Swift data collected on the AX J1820.5–1434, a high mass X-ray binary (HMXB) discovered during the ASCA Galactic plane survey at R.A._{J2000} = 18h20m29.5s, Dec_{J2000} = –14°34′24″ with an error radius of 0.5′ (Kinugasa et al. 1998). The timing analysis of the ASCA data allowed the detection of a coherent pulsation with a period of 152.26 ± 0.04 s. The spectrum was modeled with a strongly absorbed ($N_{\text{H}} = 9.8 \pm 1.7 \times 10^{22}$ cm^{–2}) power-law with photon index $\Gamma = 0.9 \pm 0.2$ and a 6.4 keV iron line with equivalent width ~ 100 eV. The average absorbed flux was 2.3×10^{-11} erg s^{–1} cm^{–2} in the 2–10 keV energy band. The source was detected in the hard X-rays with INTEGRAL (Lutovinov et al. 2003), with an average 18–60 keV flux of ~ 9.3 erg s^{–1} cm^{–2} between March and April 2003, while the non-detections in later observations indicated its transient nature (Filippova et al. 2005). An optical counterpart was proposed by Negueruela & Schurch (2007) to be the mid or early B-type star USNO-B1.0 0754-0489829. However, thanks to a refinement of the X-ray position achieved through two later XMM-

Newton and Chandra observations (R.A._{J2000} = 18h20m30.09s, Dec_{J2000} = –14°34′23.52″ derived with Chandra, with an error circle of 0.64″, Kaur et al. 2010), this counterpart candidate was rejected because inconsistent with the new position. No optical counterpart is visible in the Digitized Sky Survey while a bright near infrared (NIR) counterpart was found in the Two Micron All Sky Survey (2MASS) at R.A._{J2000} = 18h20m30.10s, Dec_{J2000} = –14°34′22.9″ (error radius 0.1″). The J, H and Ks magnitudes of the NIR source are 15.41, 13.25 and 11.75, respectively. The bright NIR counterpart could be either an early-type single star or a blend of a few nearby stars not resolved due to poor resolution of the 2MASS observations. As a consequence, the actual counterpart of AX J1820.5–1434 remains still uncertain (Kaur et al. 2010). The spectral parameters derived from the XMM-Newton observation are consistent with those reported by Kinugasa et al. (1998), with an absorbed flux a factor of ~ 15 lower. The timing analysis confirmed the pulse period reported by Kinugasa et al. (1998). An average spin-period derivative of $(3.00 \pm 0.14) \times 10^{-9}$ s s^{–1} was determined using the previous spin-period measurement.

2. Observations and data reduction

The Swift-BAT survey data (2004/11 – 2012/03) retrieved from the HEASARC public archive¹ were processed using the BATIMAGER code (Segreto et al. 2010), dedicated to the processing of coded mask instrument data. AX J1820.5–1434 is detected with a significance of 23.6 standard deviations in the 15–150 keV all sky map, and of 24.9 standard deviations in the 15–60 keV all-sky map, where its signal-to-noise is maximized (Fig. 1, left

Send offprint requests to: A. Segreto, segreto@ifc.inaf.it

¹ <http://heasarc.gsfc.nasa.gov/docs/archive.html>

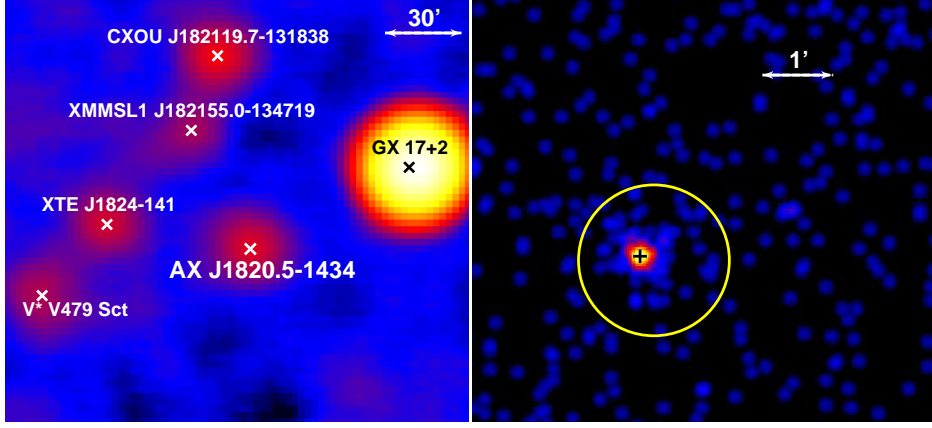


Fig. 1. **Left panel:** 15–60 keV BAT significance map of the sky region around AX J1820.5–1434. **Right panel:** 0.2–10 keV XRT image with superimposed the BAT error box (1.08 arcmin, yellow circle) and the position of the NIR counterpart (black cross) suggested by Kaur et al. (2010).

Table 1. XRT and XMM-Newton observation log.

	ObsID	T_{start} (MJD)	ΔT (s)	Exp. T (s)	Orb. phase	Rate c/s
XRT						
1	00036168001	54155.66	24404	6006	0.21	0.013
2	00037882001	55031.10	171	171	0.41	< 0.081
3	00044152001	56216.54	480	480	0.35	0.16
XMM						
Epn	0511010101	54373.29	8150	8150	0.23	0.080
EMOS1	–	–	10733	10733	–	0.025
EMOS2	–	–	10753	10753	–	0.025

Notes. ΔT is the observation length; Exp. T is the net exposure time; the orbital phase is referred to the profile in Figure 2b. The count rate reported for the Swift-XRT ObsID 00037882001 is a 3σ upper limit.

panel). The latter energy band was used to extract the light curve with the maximum resolution allowed by the Swift-BAT survey data. The background subtracted spectrum averaged over the entire survey period was extracted in eight energy channels and analyzed using the BAT redistribution matrix available in the Swift calibration database².

Two Swift-XRT observations were used in this work to perform broad band spectroscopy: ObsID 00036168001, performed on 2007 February 24, with CCD substrate voltage set at 0V and with a net exposure of 6 ksec, and ObsID 00044152001, performed on 2012 October 16, for ~ 500 s of exposure time (CCD substrate voltage set at 6V). Both pointings are in Photon Counting observing mode (Hill et al. 2004). A third observation (ObsID 00037882001, 2009 July 19) has an exposure time of only 170 s, and the source was not detected. The data were processed with standard procedures (XRTPIPELINE v.0.12.4), filtering and screening criteria, adopting a 0-12 grade selection. The source events were extracted from a circular region (20 pixel radius, with 1 pixel = 2.36 arcsec) centered on the source centroid, determined using the task XRTCENTROID ($R.A._{J2000} = 18^{\text{h}}20^{\text{m}}30.1^{\text{s}}$, $\text{Dec}_{J2000} = -14^{\circ}34'23.8''$, with 90% confidence region of 3.98'' radius). Figure 1 (right panel) shows the XRT image with the position of the NIR counterpart, that is offset with respect to the XRT source of 0.9''. The background for the spectral analysis was extracted from an annular region with inner and outer radii 30 and 70 pixels, respectively. XRT ancillary response file were generated with XRTMKARF³; we used the spectral

redistribution matrix v011 for ObsID 00036168001 and v013 for ObsID 00044152001. The spectral analysis was performed using XSPEC v.12.5. The event arrival times were corrected to the SSB using the task BARYCORR⁴.

We also extracted the XMM-Newton spectrum of the source, from the same pointings whose analysis was performed in Kaur et al. (2010). We extracted both Epic-PN and MOS spectra, using standard pipelines of SAS tools. We selected a circular region of 10 arcsec radius centered on the source position for source spectra and a similar region from a nearby source-free area for the background spectra. We checked the consistency of our analysis by successfully reproducing the best-fitting model of Kaur et al. (2010).

3. Timing analysis

A folding timing analysis (Leahy et al. 1983) was applied to the 15–60 keV Swift-BAT light curve searching for the presence of periodic modulations with period between 0.5 and 500 d. **The method consists in building a light curve profile at different trial periods by folding the photon arrival times in N phase bins. For each resulting light curve the χ^2 with respect to the average count rate is evaluated: a periodic pulsation corresponds to a large value of χ^2 .** The resolution of the period search is $\Delta P = P^2/(N\Delta T)$, where P is the trial period, $N = 16$ is the number of phase bins used to build the trial profile, and $\Delta T = 228$ Ms is the data time span. The profile for each trial period was built weighting the rates by the inverse square of the corresponding statistical error (see Cusumano et al. 2010). This allows to cope with the large spread of statistical errors that characterizes the Swift-BAT survey data, mainly due to the wide range of off-axis directions in which the source is observed. The resulting periodogram (Figure 2a) shows several features emerging over the noise: the one with the shortest period is at $P_0 = 54.0 \pm 0.4$ d ($\chi^2 \sim 254$), where P_0 and its error are the centroid and the standard deviation obtained modeling this feature with a Gaussian function, while the other features result to be multiples of P_0 . The intensity profile (Fig. 2b) obtained by folding the data at P_0 with $T_{epoch} = 54684.809$ MJD shows a large asymmetric single peak profile with a minimum which is marginally consistent with zero emission. For larger values of

² <http://swift.gsfc.nasa.gov/docs/heasarc/caldb/swift/>

³ <http://heasarc.gsfc.nasa.gov/ftools/caldb/help/xrtmkarf.html>

⁴ <http://heasarc.gsfc.nasa.gov/ftools/caldb/help/barycorr.html>

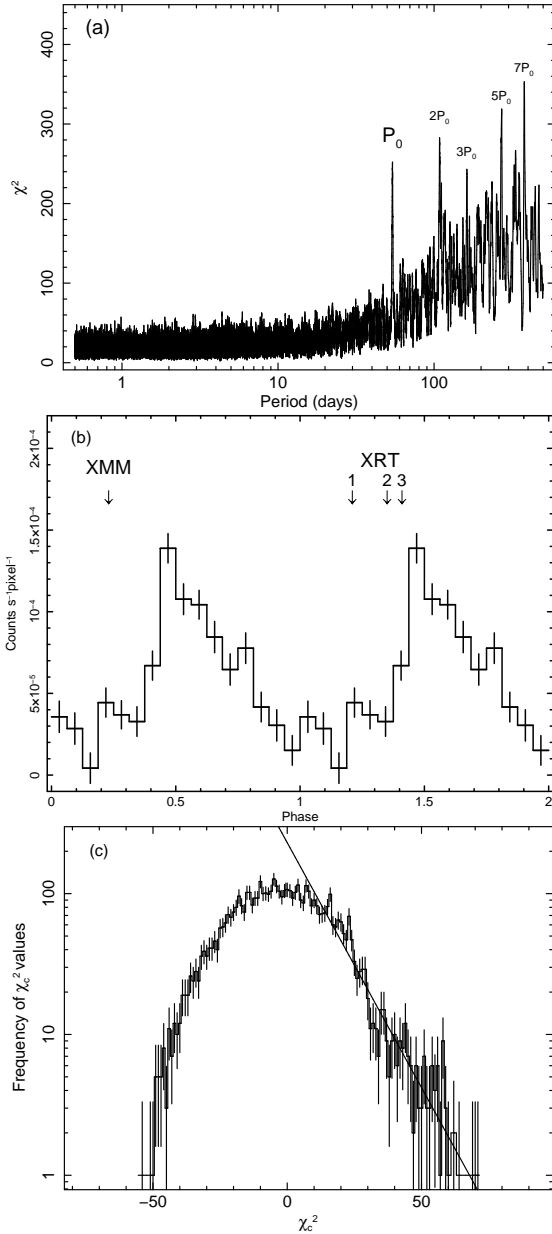


Fig. 2. **a:** Periodogram of *Swift*-BAT (15–60 keV) data for AX J1820.5–1434. **b:** Light curve folded at a period $P_0 = 54.0$ d, with 16 phase bins. The arrows mark the orbital phase of the Swift-XRT and XMM-Newton observations. **c:** Histogram distribution of the χ_c^2 values; the solid line is the exponential function that best fits the right tail of the distribution.

the trial period the periodogram shows the typical average χ^2 increase which is expected when the source emission is characterized by long term time variability (red noise). In presence of red noise the χ^2 statistics cannot be applied and the significance of the feature is to be evaluated with respect to the local noise fluctuation of the periodogram. Thus we fit the periodogram with a second order polynomial and subtract the best fit trend from the χ^2 values, obtaining a “corrected” periodogram χ_c^2 . The value of χ_c^2 at P_0 is ~ 194 .

In Fig 2c we show the histogram built from the corrected periodogram selecting the values in the period interval between 24 and 104 d (as this interval is characterized by a noise level quite consistent with the noise level at P_0) and excluding those falling

in an interval of $\pm\Delta P_0$ around P_0 . We then use an exponential function to extrapolate the histogram right tail and compute its area for $\chi_c^2 > \chi_c^2(P_0) = 194$. Normalizing this value to the total area of the histogram we obtain 1.0×10^{-7} that represents the probability of random occurrence for $\chi_c^2 > 194$. This corresponds to a significance of 5.4 standard deviations in Gaussian statistics.

Figure 3 shows the 15–60 keV light curve of AX J1820.5–1434 with a bin time of $P_0/6 = 9.0$ d. The vertical shaded bars mark the phase interval 0.44–0.62 of Figure 2b. In $\sim 50\%$ of the cycles we observe a significant intensity enhancement in this phase interval. The source shows also a few episodes of significant intensity enhancements at different phases. The Swift-XRT observations correspond to a phase interval between 0.2 and 0.4 in Figure 2b. The variations of the rate observed among the observations (Table 1) are in fair agreement with the shape of the Swift-BAT folded profile with the highest rate observation (ObsID 00044152001) corresponding to the profile peak. The statistic content of the Swift-XRT observations is too low (~ 70 counts in observations 1 and 3) to see the modulation of ~ 152 s reported by Kinugasa et al. (1998) and confirmed by Kaur et al. (2010) with the XMM-Newton data.

4. Spectral analysis

Before performing a broad band spectral analysis we checked the range of spectral variations observed in the available data sets. The spectra of the two Swift-XRT pointed observations where AX J1820.5–1434 is detected (see Sect. 2) and of the XMM observation were fitted simultaneously with an absorbed power law and constraining the absorption column density and the photon index to be the same for both data set. The residuals resulting from the best fit model were consistent with each other within the errors. The absorption column density was $11.3^{+2}_{-2} \times 10^{22} \text{ cm}^{-2}$ while the photon index was $1.6^{+0.3}_{-0.3}$. The same check was done on the Swift-BAT spectra produced dividing the BAT data into four 22-month long time intervals and into three different orbit phase intervals (0.375–0.4375 plus 0.625–0.875, 0.4375–0.625 and 0.875–1.375, see Figure 2b), that were fitted with a power law. As for the Swift-XRT spectra, the photon index was tied to be the same in the three datasets. The best fit residuals show the same trend for all the BAT datasets with a best fit photon index of $2.6^{+0.1}_{-0.1}$.

The broad band spectral analysis was therefore performed coupling the 15–150 keV BAT spectrum averaged over 88 months, the two Swift-XRT spectra and the XMM-Newton spectra. In order to take into account flux variations and intercalibration issues, we included in the model a multiplicative normalization factor, fixed to 1 for the Swift-XRT spectrum of Obs ID 00044151001 and left free for all the other spectra. A strongly absorbed ($N_H \sim 1.7 \times 10^{23} \text{ cm}^{-2}$) power law was **adequate** to describe the data with an acceptable χ^2 of 158.4 (182 d.o.f.). Figure 4 shows data, best fit model and residuals. Table 2 reports the best fit parameters (quoted errors are given at 90% confidence level for a single parameter). We also tried a model consisting in an absorbed power-law with a high energy exponential cutoff (phabs*cutoffpl) without any significant fit improvement ($\chi^2=145.4$ with 181 d.o.f.).

5. Conclusions

The entire dataset of Swift and XMM-Newton X-ray data on AX J1820.5–1434 was analyzed to explore the temporal and

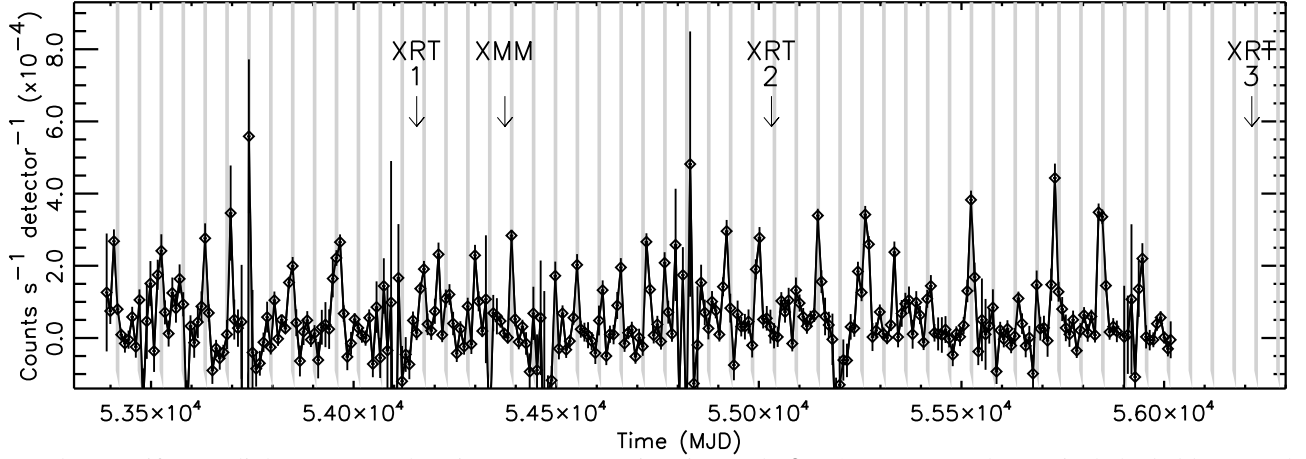


Fig. 3. 15–60 keV Swift-BAT light curve. Each point represents a time interval of $P_0/6 = 9.0$ d. The vertical shaded bars mark the phase interval 0.44–0.62 of the folded profile in Figure 2b. The arrows mark the epoch of the Swift-XRT and XMM-Newton observations. The third Swift-XRT observation is later than the 88-month BAT survey data analysed in this paper.

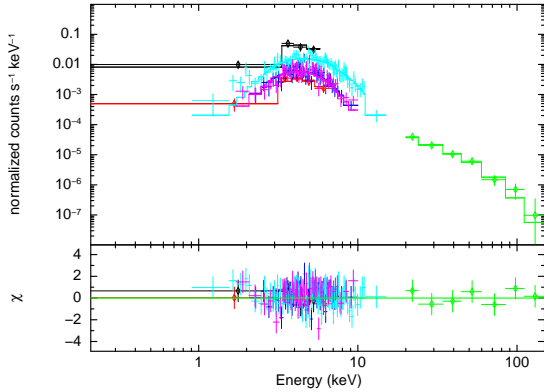


Fig. 4. AX J1820.5–1434 broad band (0.2–150 keV) spectrum. **Top panel:** XRT (black and red data), EPIC-pn (cyan data), EPIC-MOS1 and EPIC-MOS2 (magenta and blue data), BAT data (green data) and best fit $\text{phabs}^*(\text{powerlaw})$ model. The Swift data are marked with diamonds. **Bottom panel:** Residuals in unit of standard deviations.

Table 2. Best fit spectral parameters.

Parameter	Power law	Units
n_{H}	$1.69^{+0.17}_{-0.15} \times 10^{23}$	cm^{-2}
Γ	$2.44^{+0.15}_{-0.14}$	
N	$4.6^{+2.0}_{-1.4} \times 10^{-2}$	$\text{ph}/(\text{keVcm}^2\text{s}) @ 1 \text{ keV}$
C_{V0}	$0.09^{+0.04}_{-0.03}$	
C_{BAT}	$0.8^{+0.04}_{-0.03}$	
C_{EPIC}	$0.06^{+0.02}_{-0.01}$	
$F_{0.2-10 \text{ keV}}$	$2.2^{+0.4}_{-0.3} \times 10^{-10}$	$\text{erg s}^{-1} \text{cm}^{-2}$
$F_{15-150 \text{ keV}}$	$4.1^{+0.05}_{-1.25} \times 10^{-11}$	$\text{erg s}^{-1} \text{cm}^{-2}$
χ^2	158.4 (182)	

Notes. C_{V0} , C_{EPIC} and C_{BAT} are the constant factors to be multiplied to the model to match the Swift-XRT data collected with CCD substrate voltage set to 0 Volt, EPIC data and BAT data, respectively. The constant factors relevant to the three EPIC detectors set to the same best fit value for the three datasets. We report unabsorbed fluxes for the characteristic Swift-XRT (0.2–10 keV) and BAT (10–150 keV) energy bands.

spectral properties of the source. The timing analysis performed on the 88-month BAT survey data unveiled a periodic intensity modulation at $P_0 = 54.0 \pm 0.4$ d, with a significance higher than 5.4 standard deviations in Gaussian statistics. Interpreting this long periodicity as the orbital period of the binary sys-

tem, and knowing the spin period (Kinugasa et al. 1998) of the compact star, we have located the source position on the Corbet diagram (Corbet 1986). The source lays in the plot region populated by Be/X-ray binaries (Fig. 5). The BAT light curve with a time bin of $P_0/6$ shows periodic intensity enhancements mostly concentrated in a narrow phase interval ($\lesssim P/6$). However, some of them have a longer time duration, and together with a few enhancement episodes that seems to be not related to the same phase interval, this explains the asymmetric triangular peak spanning about 50% of the orbital period in the BAT light curve folded at P_0 . This suggests that the accretion onto the compact object is not strictly related to the periastron passage, as typical for highly eccentric Be/X-ray binaries. The lack of information on the companion star type prevents us from further investigation on the orbital parameters of the system. If the counterpart of AX J1820.5–1434 proposed by Kaur et al. (2010) is not a blend of objects but rather a single source, we can consider its NIR magnitudes and assume the intrinsic colors typical of late O/early B-type stars (Wegner 1994): we find a color excess $E(J - K) \sim 3.5$ mag, that implies a reddening $A_V \sim 21$ mag using the Milky Way extinction law of Cardelli et al. (1989) and assuming the total-to-selective extinction ratio of Rieke & Lebofsky (1985). Although it is known that the N_{H} can vary on short scales throughout the Galactic Plane, and the value of the gas-to-dust ratio is not universal in the Galaxy, we can nevertheless use this approach to get an (admittedly rough) estimate of the Galactic line-of-sight hydrogen column density towards AX J1820.5–1434. This large extinction naturally explains the lack of detection of an optical counterpart for this source and, from the formula of Predehl & Schmitt (1995), it implies a column density of $\sim 3.8 \times 10^{22} \text{ cm}^{-2}$, substantially lower than that inferred from our X-ray spectral analysis and again pointing to the presence of further absorbing material local to the system. Assuming this amount of reddening along the AX J1820.5–1434 line of sight and a B0 spectral type for the companion star in this system, we can infer its distance depending on the luminosity class of the star. We consider the main sequence and giant cases (luminosity classes V and III, respectively), as the location of the source in the Corbet diagram tends to rule out the presence of an early supergiant in this system. From the tabulated absolute magnitudes for this type of stars (Lang 1992) we find distances of ~ 3.5 and ~ 6.0 kpc for the main sequence and the giant companion case, respectively. This range

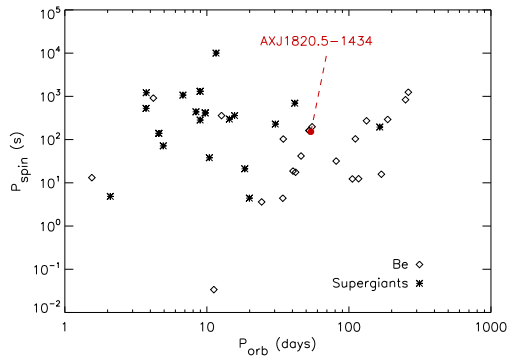


Fig. 5. Corbet diagram for HMXBs with known spin and orbital period. Diamond and star points represent the Be and supergiant systems, respectively. The red filled circle marks the position of AX J1820.5–1434.

of distance implies a 0.2–10 keV (15–150 keV) luminosity range of $3.2 \times 10^{35} - 9.5 \times 10^{35} \text{ erg s}^{-1}$ ($6.0 \times 10^{34} - 1.8 \times 10^{35} \text{ erg s}^{-1}$).

The set of XMM-Newton, Swift-XRT and Swift-BAT data allows for a broad band spectral analysis in the 0.2–150 keV energy band. The data can be described with a strongly absorbed ($N_{\text{H}} \sim 1.7 \times 10^{23} \text{ cm}^{-2}$) power law with photon index $\Gamma \approx 2.44$. We have modified the power law by a high energy cutoff, but the cutoff energy we obtain is poorly constrained and the statistical improvement is not significant.

Acknowledgements. We thank the referee R. Walter whose comments helped to improve the paper. This work has been supported by ASI grant I/011/07/0.

References

- Barthelmy, S. D., et al. 2005, *Space Science Reviews*, 120, 143
 Cardelli, J.A., Clayton, G.C., & Mathis, J.S. 1989, *ApJ*, 345, 245
 Corbet, R. H. D. 1986, *MNRAS*, 220, 1047
 Corbet, R. H. D., & Krimm, H. A. 2009, *The Astronomer’s Telegram*, 2008, 1
 Corbet, R. H. D., Krimm, H. A., & Skinner, G. K. 2010, *The Astronomer’s Telegram*, 2559, 1
 Cusumano, G., La Parola, V., Romano, P., et al. 2010, *MNRAS*, 406, L16
 D’Ai, A., La Parola, V., Cusumano, G., et al. 2011, *A&A*, 529, A30
 Filippova, E. V., Tsygankov, S. S., Lutovinov, A. A., & Sunyaev, R. A. 2005, *Astronomy Letters*, 31, 729
 Kinugasa, K., Torii, K., Hashimoto, Y., et al. 1998, *ApJ*, 495, 435
 Gehrels, N., et al. 2004, *ApJ*, 611, 1005
 Hill, J. E., Burrows, D. N., Nousek, J. A., et al. 2004, *Proc. SPIE*, 5165, 217
 Lang, K. R. 1992, *Astrophysical Data I. Planets and Stars*, X, 937 pp. 33 figs., Springer-Verlag Berlin Heidelberg New York
 La Parola, V., Cusumano, G., Romano, P., et al. 2010, *MNRAS*, 405, L66
 Lebrun, F., Leray, J. P., Lavocat, P., et al. 2003, *A&A*, 411, L141
 Leahy, D.A., Darbro, W., Elsner, R.F. et al. 1983, *ApJ*, 266, 160
 Lutovinov, A., Walter, R., Belanger, G., et al. 2003, *The Astronomer’s Telegram*, 155, 1
 Kaur, R., Wijnands, R., Paul, B., Patruno, A., & Degenaar, N. 2010, *MNRAS*, 402, 2388
 Negueruela, I., & Schurch, M. P. E. 2007, *A&A*, 461, 631
 Predehl, P. & Schmitt, J.H.M.M. 1995, *A&A*, 293, 889
 Rieke, G. H., & Lebofsky, M. J. 1985, *ApJ*, 288, 618
 Segreto, A., Cusumano, G., Ferrigno, C., La Parola, V., Mangano, V., Mineo, T., & Romano, P. 2010, *A&A*, 510, A47
 Ubertini, P., Lebrun, F., Di Cocco, G., et al. 2003, *A&A*, 411, L131
 Wegner, W. 1994, *MNRAS*, 270, 229
 Winkler, C., Courvoisier, T. J.-L., Di Cocco, G., et al. 2003, *A&A*, 411, L1